Journal of Applied Polymer Science

Mechanical properties and stem cell adhesion of injection-molded poly(ether ether ketone) and hydroxyapatite nanocomposites

Bruna Turino Rego,[1] Wilson Alves Ribeiro Neto,[1] Ana Claudia Chagas de Paula,[2] Alfredo Miranda Góes,[2] Rosario Elida Suman Bretas[1]

[1]Department of Materials Engineering, Universidade Federal de São Carlos, Rodovia Washington Luís, Km 235, PO Box 676, São Carlos Sao Paulo 13565-905, Brazil

[2]Institute of Biological Science, Universidade Federal de Minas Gerais, Pampulha, Belo Horizonte Minas Gerais, Brazil

Correspondence to: R. E. S. Bretas (E-mail: bretas@ufscar.br)

ABSTRACT: A nanocomposite of poly(ether ether ketone) (PEEK) with 10 wt % hydroxyapatite (HA) was produced by extrusion and injection molding. Afterward, the samples were thermally treated. Thermal and short- and long-term mechanical characterizations of the samples were made. The adhesion of human adipose stem cells (h-ASCs) on the samples was also monitored. The ultimate tensile strength (UTS) and elastic modulus values of the nanocomposite were found to be much higher than those of trabecular bone. The impact strength of PEEK was not modified by HA; this suggested that there was no formation of large agglomerates of nanoparticles that could concentrate the stresses. With regard to fatigue life, both the thermally and nonthermally treated nanocomposites did not fail after 10^6 cycles when maximum stresses of 30 and 50% of the UTS were applied, but they failed when the maximum applied stress was 75% of the UTS and behaved as cortical bone. After 5 days of culturing, the h-ASCs had a higher proliferation in the nanocomposite than in pure PEEK because of the presence of HA. © 2014 Wiley Periodicals, Inc. J. Appl. Polym. Sci. **2015**, *132*, 41748.

KEYWORDS: biomedical applications; composites; mechanical properties

Received 19 March 2014; accepted 13 November 2014

DOI: 10.1002/app.41748

INTRODUCTION

Poly(ether ether ketone) (PEEK) is a semicrystalline polymer with a high mechanical strength and high chemical and thermal stability;[1,2] it has been mostly used as an engineering polymer. Because of its outstanding properties and because it is radiolucent to X-rays and nontoxic to living cells, its use as a biomaterial has been investigated for orthopedics, spinal implants,[3–5] and in neurosurgery.[6] However, its bio-inertness and hydrophobic surface are unfavorable for osteoblast cell adhesion, and thereby, it has unsatisfactory osteointegration capabilities when it is used as a bone implant in the human body.[4] One way to overcome these drawbacks is to modify its surface with plasma treatment, etching, or the addition of hydrophilic biofillers, among others.

Biomaterials in the form of polymeric composites and nanocomposites are widely used because of the synergistic combination of the high mechanical strength of the filler (usually a ceramic or a metal) with the optimal viscoelastic properties of the polymeric matrix.[7] In orthopedic applications, for instance, the use of these composites is widespread because of their low density, high performance, and mechanical properties, which are similar to those of bone tissue.

Hydroxyapatite (HA) is the main inorganic component of bones and teeth. It can also be chemically synthesized because it has osteo-induction properties; that is, it is capable of promoting the growth of a new bone tissue on an implant from the tissues surrounding it and, thus, stabilizes the implant in a short period.[8,9]

The particles of HA usually have nanometric dimensions, depending on the synthesis method. However, when it is added to PEEK, the mechanical properties of the PEEK composites are usually compromised because of the poor physical bonding between PEEK and HA, which form agglomerates of microdimensions.[10] Thus, to produce nanocomposites with optimal properties, the agglomerates should be dispersed with methods that must overcome the high interaction forces between the nanoparticles.

The use of nanocomposites as biomaterials has enormous potential; it is well known that inorganic nanoparticles, such as nano-Al_2O_3 and nano-SiO_2, develop a strong bonding between them and the polymeric matrix. This improves the mechanical properties of the nanocomposite.[11] It has also been shown that osteoblasts cells have better interactions on nanophase ceramics.[12–15] For that reason, it is predictable that nanoparticles of HA may play a similar role in strengthening bonding with the PEEK matrix and, consequently, may produce a

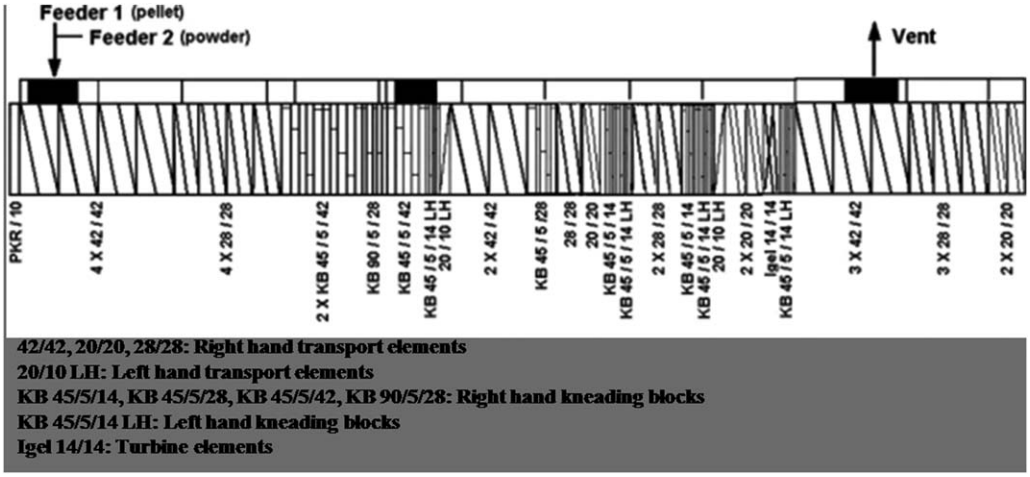

Figure 1. Screw profile of the twin extruder.[24]

nanocomposite with excellent mechanical properties and a high bioactivity.[11] However, it is still very difficult to promote the dispersion and distribution of the nanoparticles through the viscoelastic polymer with standard mixing procedures in the melt state.[16] The addition of a high amount of HA (>20 wt %) to PEEK increases the elastic modulus (E) and promotes the bioactivity of the composite; however, the ultimate tensile strength (UTS) and toughness decrease.[8,17] Other works,[11,18] in which nanocomposites of PEEK with HA were prepared by injection molding, showed that the tensile strength of the nanocomposites increased with the amount of HA (≤5 vol %) but decreased when the concentration was above 10 vol %. This was probably due to HA agglomeration. The authors also observed that the HA nanoparticles had strong bonding to PEEK when they were well dispersed; also, no debonding was observed between both components. Another pioneering work of the same team[19] produced PEEK/HA nanocomposites by the *in situ* polymerization of PEEK; the authors found that the tensile strength of the 2.6 vol % nanocomposite was high because of the strong interfacial bonding between the polymer and filler as result of *in situ* polymerization.

It is known that the addition of low concentrations (3–5 wt %) of nanoparticles to a polymeric matrix can improve the properties of standard composites with the addition of 20–30 wt % microparticles. However, to obtain this improvement, it is necessary that the concentration of nanoparticles be above the percolation threshold; that is, it is necessary that a percolated network of individual nanoparticles be formed through the polymer.[20] Usually, above this concentration, a gain in mechanical properties is expected. This percolation threshold depends on the aspect ratio L/D (where L is the length and D is the diameter) of the particles and is lower as L/D increases.[21] Thus, nanoparticles such as carbon nanotubes or lamellar montmorillonites (MMTs), because of their high L/D, have very low percolation thresholds. However, for spherical particles, this threshold is high, approximately 29 vol %, as predicted by Lorenz and Ziff.[22] This would correspond to approximately 50 wt % in the case in which the spherical HA nanoparticles were added to PEEK. The dispersion and distribution of this high amount of particles in PEEK, however, it would require the use of nonconventional and high-energy processing methods.

Thus, in this study, nanocomposites of PEEK/HA were produced by twin-screw extrusion followed by injection molding; the nanocomposites had their microstructure and thermal behavior characterized, their short- and long-term mechanical properties measured, and their *in vitro* biocompatibility tested.

EXPERIMENTAL

Materials

PEEK (Ketaspire KT-880 NT, Solvay Advanced Polymers) was chosen as the matrix of the nanocomposites. According to the supplier, this resin had a density of 1.30 g/cm^3, a melt flow index of 36 g/10 min (400°C/2.16 kg), a glass-transition temperature (T_g) of 147°C, and a melting temperature (T_m) of 343°C.

The nanoparticle used was HA (product #677418, from Sigma-Aldrich), with a surface area higher than 9.4 m^2/g and the chemical formula $[Ca_5(OH)(PO_4)_3]_x$. The particle size distribution was already calculated,[23] and it was found that approximately 66% of the particles had diameters lower than 100 nm and that the weight-average diameter of the HA particle was 94.9 nm and the number-average diameter was 105 nm.

Processing of the Nanocomposite

A nanocomposite of PEEK and 10 wt % HA was produced. This concentration of HA was well below the theoretical percolation concentration (~50 wt %); therefore, no formation of a percolated network was expected. This low concentration of HA was chosen because of its high cost. Also, no compatibilizing agents were used in this study because we assumed that the polar surface of HA could interact with the polar groups of PEEK. In addition, because of the high T_m of PEEK, finding a compatibilizing agent that would withstand this high temperature was difficult.

The nanocomposite was produced in a corotational twin-screw extruder from Werner-Pfleider (model ZSK30) with a diameter of 30 mm and a length of 1070 mm. The screw profile was the same as that used in another work of ours[24] for the production of poly (amide) 6 (PA6) and MMT nanocomposites because as

Table I. Molding Conditions

Condition	Q (cm^3/s)	P_{emp} (Bar)	T_w (°C)
1	10	580	96
2	35	580	96
3	55	580	96

PA6 and PEEK had low melt viscosities and broad Newtonian plateaus, their dispersion capacities were probably similar. The screw profile is shown in Figure 1. Beatrice *et al.*[24] calculated the shear rates for this screw profile. At 120 rpm, the shear rate at the transport elements was 30 s^{-1}, whereas the shear rate at the kneading blocks was approximately 1900 s^{-1}.

PEEK was powdered with a cryogenic mill (Micron Powder Systems, model Mikro-Bantam). Subsequently, it was mixed with HA, and the dried mixture was fed into the twin-screw extruder through feeder number 2. The extrusion flow rate (Q) was 4 kg/h at 120 rpm. The heating profile of the extruder was as follows: Zone 1 (feed zone) = 340°C, Zone 2 = 380°C, Zones 3 and 4 = 365°C, and Zones 5 and 6 = 360°C. The mixing average torque was 55%. Preliminary torque rheometer tests showed that at this temperature and residence time, no thermal degradation of PEEK (which could occur by branching and curing[25]) occurred.

The extruded nanocomposite was named 90/10-ext. Subsequently, the pure PEEK and the 90/10-ext nanocomposite were injection-molded in an Arburg 270 V machine with the application of a clamp force of 300 kN and a screw diameter of 25 mm coupled to a cooling/heating unit from HB THERM (model HBW140). Samples for tension and impact tests following ASTM D 638 and ASTM D 256 standard procedures were produced.

The materials were injected at three conditions with only the injection flow rate Q varied, as shown in Table I. These processing parameters were chosen to obtain samples without defects.[26]

The limits of Q were chosen according to the recommendation of the supplier. The mold temperature (T_w) was kept at 96°C because water was the cooling medium of the cooling unit. Because this last temperature was well below the T_g of PEEK and the cooling temperatures recommended by the supplier were between 177 and 204°C, the samples were annealed after injection molding in an oven at 210°C for 5 h to improve their crystallinity. The packing pressure (P_{emp}) was fixed at 580 bars to prevent short shots and sink marks. Under all of the molding conditions, the packing and cooling times were kept at 10 and 20 s, respectively. The temperature profile along the injection screw was 365/370/380/385/390°C. The samples were named as shown in Table II.

Characterization of the Nanocomposites

Thermogravimetric Analysis (TGA). The thermal stability of the nanocomposites was measured in an instrument from TA Instruments (model Q50) at a heating rate of 20°C/min from room temperature up to 800°C under a nitrogen atmosphere.

Differential Scanning Calorimetry (DSC). T_m, the crystallization temperature (T_c), and the crystallinity index of the samples (X_{c_DSC}) were measured with equipment from TA Instruments (model QS100) under a nitrogen atmosphere. The following thermal cycles were used:

1. Heating from 20 to 400°C at a heating rate of 10°C/min and held for 3 min at this last temperature to erase the thermal history of the sample. In this interval, T_m and X_{c_DSC} were measured.
2. Cooling from 400 to 20°C at a cooling rate of 10°C/min to determine the crystallization range. In this interval, T_c was measured.
3. Heating again from 20 to 400°C at 10°C/min.

X_{c_DSC} (%) was measured using small amounts of material cut along the thickness of the samples and it was calculated from eq. (1):

$$X_{C_{DSC}}(\%) = \frac{\Delta H_f - \Delta H_{CC}}{W_f \Delta H_f^0} \times 100\%. \quad (1)$$

where ΔH_f is the heat of melting of the sample, ΔH_{cc} is the heat of cold crystallization, W_f is the mass fraction of PEEK in the nanocomposite, and ΔH_f^0 is the equilibrium heat of melting of PEEK, equals to 130 J/g.[27]

Microstructural Characterization. The distribution of the nanoparticles through the PEEK matrix was analyzed by scanning electron microscopy (SEM; Philips model XL30FEG) operated at 15 kV with a working distance of 10 mm.

Polarized Light Optical Microscopy (PLOM). The morphology of the injection-molded samples was analyzed by PLOM; slices of 10 μm were cut through the thickness of the samples. The cutting was made with a MICROM microtome (model HM 360) at a velocity of 6 mm/min at room temperature. The slices were analyzed with PLOM (Leica, model DMRXP, to which a Zeiss camera, model AxioCam ERc5s, was attached).

Wide-Angle X-ray Diffraction (WAXD). To observe the effect of the annealing on the crystallinity of the injection-molded samples, WAXD was made on the surface of the samples with a Rigaku diffractometer (model Ultima IV) with Cu Kα

Table II. Sample Nomenclature

Sample	Amount of HA (wt %)	Injection condition	Annealing treatment
PEEK-1	0	1	No
PEEK-2	0	2	No
PEEK-3	0	3	No
NANO-1	10	1	No
NANO-2	10	2	No
NANO-3	10	3	No
PEEK-1-TT	0	1	Yes
PEEK-2-TT	0	2	Yes
PEEK-3-TT	0	3	Yes
NANO-1-TT	10	1	Yes
NANO-2-TT	10	2	Yes
NANO-3-TT	10	3	Yes

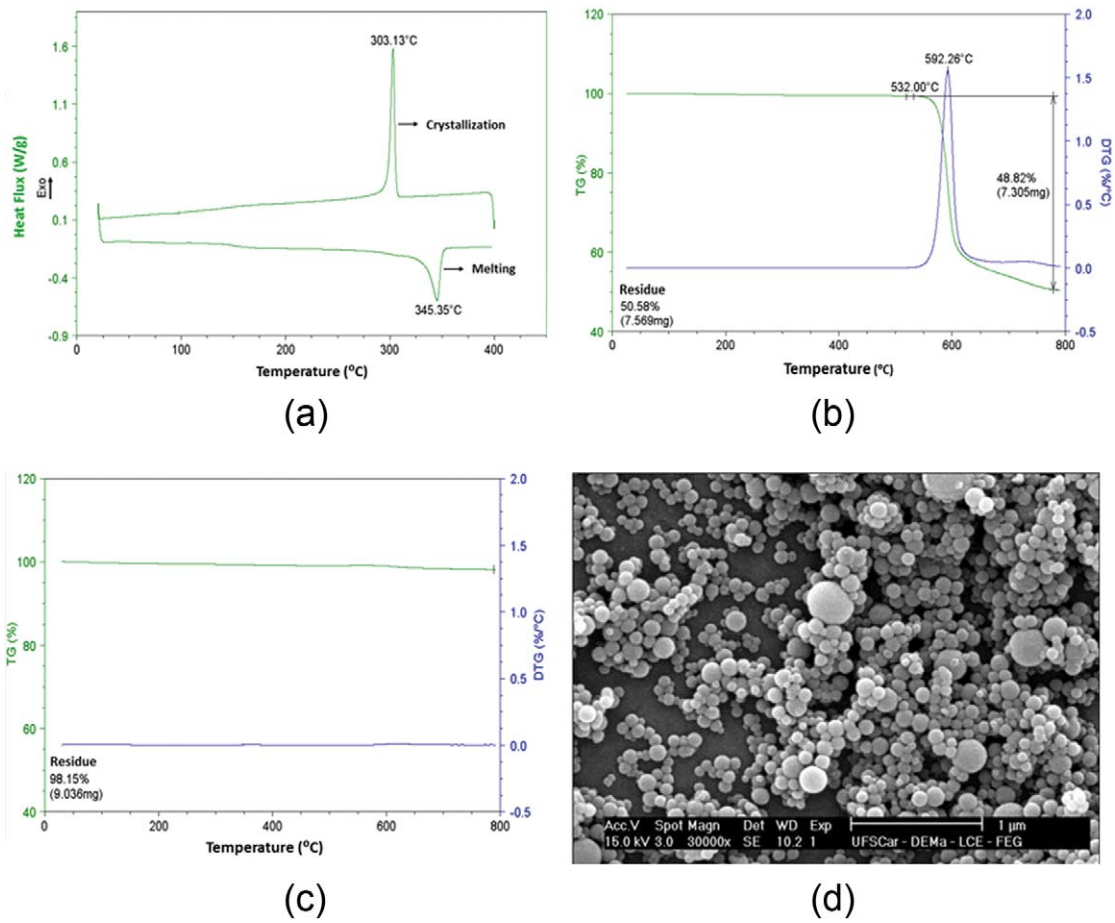

Figure 2. (a) DSC thermogram of PEEK, (b) TGA of PEEK, (c) TGA of HA, and (d) SEM of the HA particles. [Color figure can be viewed in the online issue, which is available at wileyonlinelibrary.com.]

($\lambda = 1.542$Å) and operating at 40 kV and 40 mA at a scanning rate of 1°/min.

Mechanical Characterization. The tension tests of the injection-molded samples were made in an Instron testing machine (model 5569) according to ASTM D 638 with type I samples at a rate of 5 mm/min. A strain gauge was used to obtain *E*.

The Izod impact strength of the injection-molded samples was measured in a CEAST testing machine with a 1-J hammer according to ASTM D 256. The V notches of the samples were also done in the CEAST equipment.

Fatigue tests were also done with a MTS Bionix Servohydraulic Test System in tension–tension mode and were stress controlled with sine wave form at a frequency of 10 Hz at room temperature and a value of stress ratio R = 0.1. R was defined as:

$$R = \sigma_{min}/\sigma_{max}$$

where σ_{min} and σ_{max} are the minimum and maximum applied stresses, respectively. The values of σ_{max} in each cycle to obtain the stress versus number of cycles to failure curves (SN curves) were determined from the tension tests and were equivalent to 30, 50, and 75% of the UTS of the materials. A limit for failure of 10^6 cycles was established; that is, when 10^6 cycles were attained, and the sample did not fail, the test was stopped. Three samples for each stress level for each material were tested. The temperature of the samples during the tests was monitored with an IR thermometer from Minipa (model MT-350).

Dynamic Mechanical Analyses. The dynamic mechanical properties of the samples were measured in a TA Instruments equipment (model Q800) on bending with a single-cantilever geometry, strain amplitude of 20 μm, frequency of 1 Hz, between 30 and 280°C at a heating rate of 3°C/min. Both the bending storage modulus (E') and the bending loss modulus (E'') were thus measured.

Cell Adhesion

The procedures for obtaining human adipose stem cells (h-ASCs) were already described in a recent work of ours.[23] To optically observe the cell growth, the h-ASCs were cultivated in basal culture medium in a plate with 24 wells (NUNC) at a density of 5×10^5 cells/well for 5 days at 37°C with 5% CO_2. The injection-molded samples (condition 2) of PEEK and PEEK/HA were immersed in each well in triplicate; after 5 days, the samples were fixed with glutaraldehyde (2 wt %) and phosphate-buffered saline (PBS; 0.1*M*, pH 7.4) for 6–12 h and washed three times with PBS (0.1*M*). A solution of OsO_4 in PBS (0.1*M*, 1% v/v) was used for a second fixation for 1 h. The

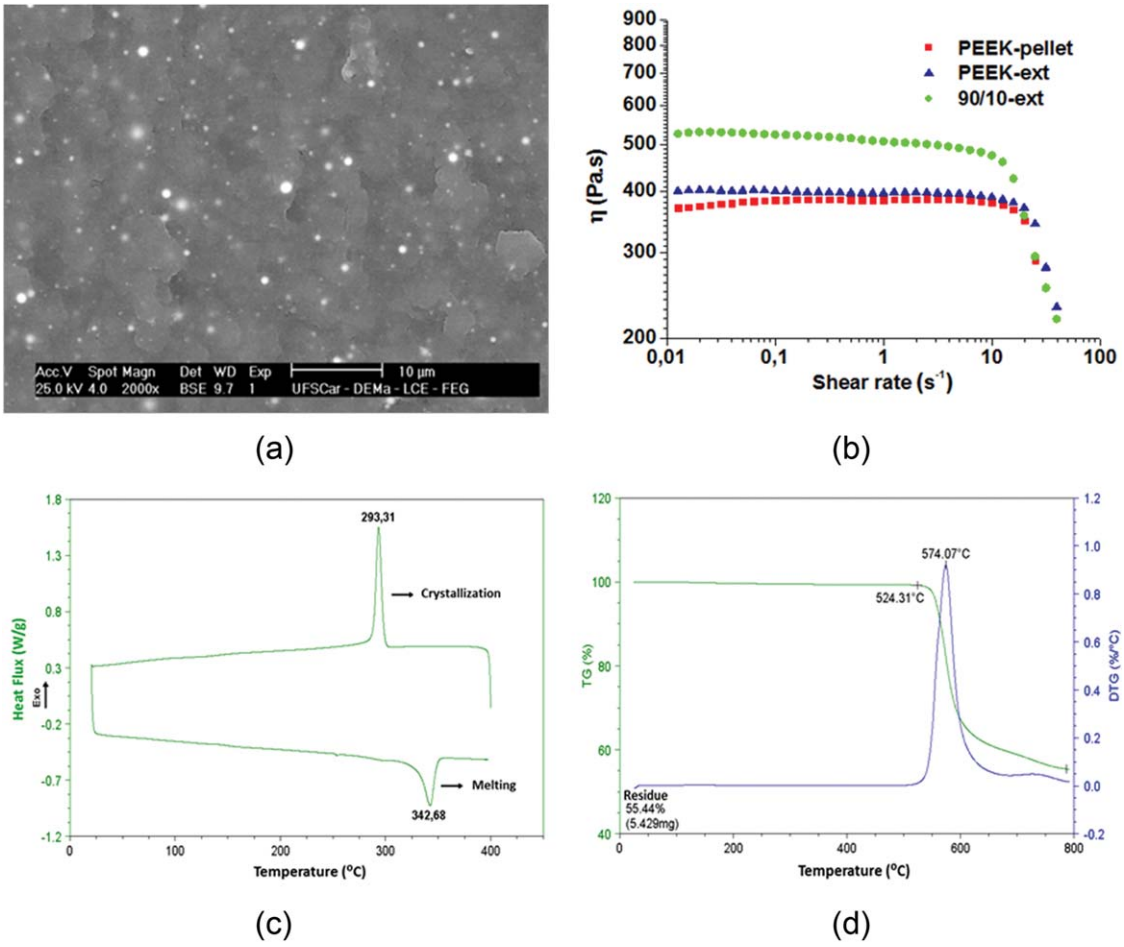

Figure 3. (a) SEM micrographs of 90/10-ext, (b) Steady-state shear viscosity (η) of the extruded samples at 360°C, (c) DSC analysis of 90/10-ext, and (d) TGA of 90/10-ext. [Color figure can be viewed in the online issue, which is available at wileyonlinelibrary.com.]

samples were washed again with distilled water and immersed in a water solution of tannic acid (1% w/v) for 20 min and washed again with distilled water. After this treatment, the samples were immersed again in a solution of 1% v/v OsO_4 for 1 h and were later washed with distilled water. The dehydration was done with alcohol at different concentrations. The dilution was made with distilled water: 30% (2×), sequentially with 50% (2×), 70% (2×), 80% (2×), and 90% (2×) and finally with concentrated alcohol at 100% (3×). After dehydration, the injection-molded samples were maintained in concentrated alcohol and dried in a critical point of CO_2. After 12 h of drying, gold metallization was done, and the samples were analyzed with the previously described SEM.

The area occupied by the h-ASCs and cellular material (proportional to the proliferation of the h-ASCs) on the surface of the injection-molded samples after 5 days was measured using SEM micrographs and the software Image-Pro Plus 6.0.

RESULTS AND DISCUSSION

PEEK and HA Characterization

Figure 2(a) shows the DSC thermogram of PEEK: T_m was 345.3°C, and T_c was 303.1°C. The melting enthalpy was 40.4 J/g; this provided an X_{c_DSC} of 31.1%. The thermal stability of PEEK was analyzed from the TGA curve, shown in Figure 2(b). The mass loss (TG %) and the derivative of the mass loss (DTG %/temperature (T)) showed that the PEEK began to lose mass at 532°C, the maximum TG % occurred at 592°C, and at 800°C, PEEK had lost almost 49% of its initial mass, leaving a non volatile residue.

With regard to HA, its thermal stability analyzed by TGA is shown in Figure 2(c); as expected, HA only lost 1.85% of water up to 800°C. The morphology of the HA nanoparticles is shown in Figure 2(d). The particles were almost spheroidal with diameters between 50 and 200 nm, as already observed.[23]

Characterization of the Nanocomposite

Characterization of the Extruded Samples. The 90/10-ext nanocomposite had a homogeneous particle distribution, as observed in Figure 3(a). The shear rates were high in the extruder; however, no degradation of the PEEK during extrusion was observed, as concluded from the similarity of the values of the shear viscosities of the extruded poly(ether ether ketone) (PEEK-ext) and the as-received PEEK pellets, shown in Figure 3(b). With regard to T_m and X_{c_DSC}, we observed that the 90/10-ext nanocomposite had a T_m of 342.6°C (similar to that of the neat PEEK) and an X_{c_DSC} of 38% (higher than that of the neat PEEK). The thermal stability of the nanocomposite was also analyzed [Figure 3(d)]; in this case, the main TG %

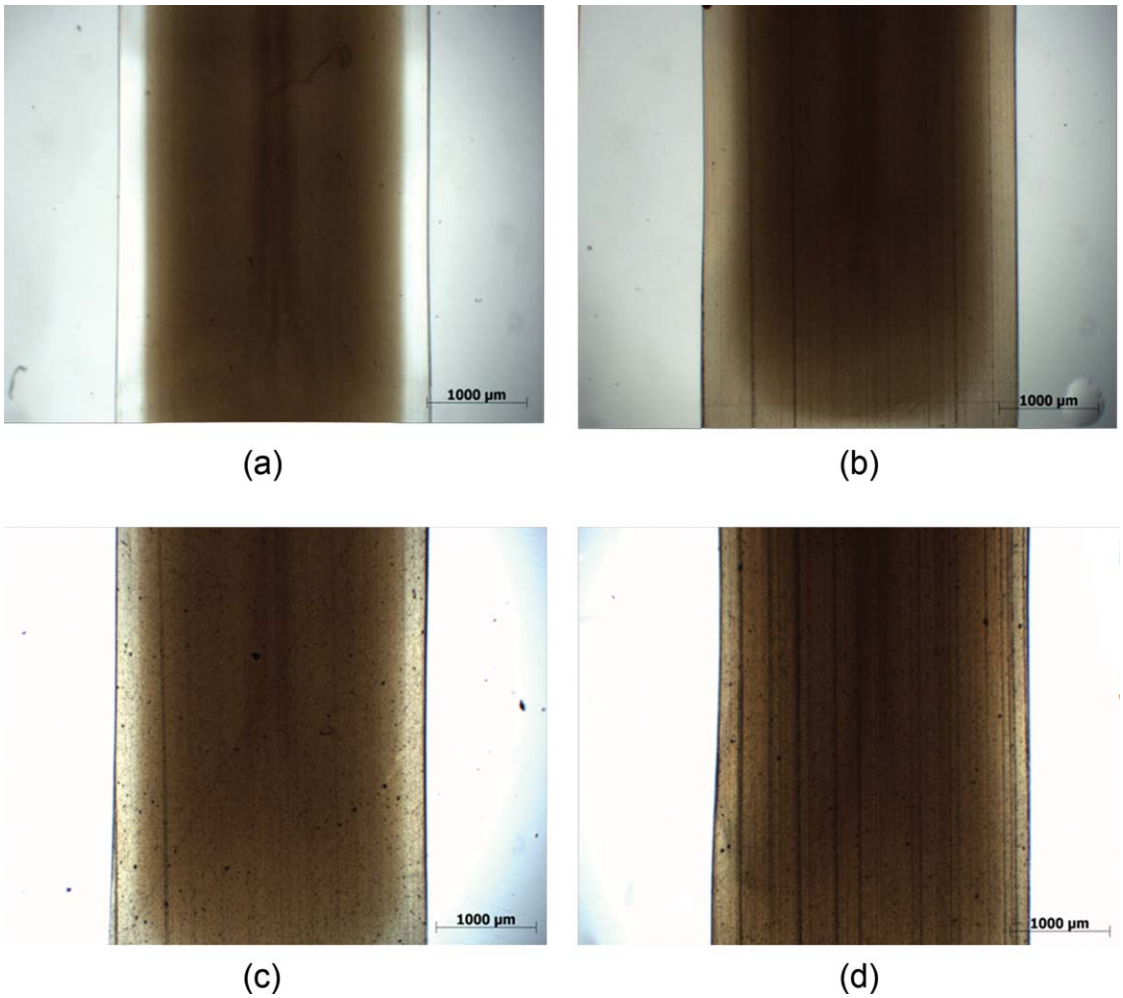

Figure 4. PLOM micrographs of the samples injection-molded under condition 2 before and after the thermal treatment: (a) PEEK-2, (b) PEEK-2–TT, (c) NANO-2, and (d) NANO-2–TT. [Color figure can be viewed in the online issue, which is available at wileyonlinelibrary.com.]

began at 524°C, that is, 8°C lower than of the pure PEEK. Thus, the 90/10-ext nanocomposite had a higher amount of crystallinity, but its crystals had a similar T_m and degradated earlier than neat PEEK. On the other hand, the T_c of the 90/10–Ext nanocomposite was 293.3°C [Figure 3(c)], which was lower than of the neat PEEK. It is worthwhile to recall that the measured T_m and X_{c_DSC} corresponded to the T_m and X_{c_DSC} of the extruded 90/10 nanocomposite, whereas the measured T_c corresponded to the crystallization temperature of the 90/10 nanocomposite after the whole deformational and thermal history from the extrusion process were erased. Thus, one explanation of this behavior could be that during the flow of the PEEK macromolecules through the extrusion die, the macromolecules were highly oriented and aligned themselves to form flow-induced nucleii (which had lower induction times as the shear rate increased, as shown by another study[28]). During the cooling stage of the extrusion process, these flow-induced nucleii, together with the HA nanoparticles [which were more thermally conductive than the PEEK and, therefore, allowed an increase in the bulk cooling rate (ΔT/Time by decreasing the time, where $\Delta T = T_m - T_c$) of the extruded nanocomposite and also probably acted as nucleating agents], made crystallization occur rapidly. Therefore, a greater number of crystals of PEEK were formed in the nanocomposite than in the pure PEEK. However, when all of the thermal history was erased in the DSC equipment, crystallization was quiescent and occurred slowly because of the low and controlled cooling rate of the equipment; therefore, it occurred later, probably because of a retardation effect in the diffusion of the PEEK macromolecules by the HA particles. Thus, the growth rate of the PEEK decreased. Other explanations are also possible, of course, in which the effect of the deformation in the extrusion die is also accounted for (flow-induced crystallization). However, to clarify the role of the HA, more DSC, PLOM, and rheological measurements should be done.[29] For example, one study of ours[29] on the crystallization of poly(trimethylene terephthalate) and MMT nanocomposite showed that during quiescent crystallization, the MMT lamellas anticipated the transition between regimes II and III of crystallization, and the process was dominated by a high nucleation rate. However, during flow-induced crystallization, we observed instead that the times for crystal growth in the nanocomposite were higher than for the pure poly(trimethylene terephthalate). These conclusions, however, are only valid for this particular nanocomposite.

Table III. Thermal Parameters and Skin Thickness of the Injection-Molded Samples

Sample	Skin (μm)	ΔH_f (J/g)	ΔH_{cc} (J/g)	X_{c_DSC} (%)	T_m (°C)	T_c (°C)
PEEK-1	252.9 ± 20.6	43.7	9.2	26.5	345.9	303.2
PEEK-2	230.1 ± 27.6	42.7	4.4	29.4	345.5	303.6
PEEK-3	174.9 ± 7.9	44.5	6.3	29.4	345.9	303.4
NANO-1	245.8 ± 26.3	42.0	8.0	29.0	346.0	291.4
NANO-2	236.7 ± 20.0	41.9	5.2	31.4	345.6	291.9
NANO-3	180.0 ± 46.9	43.4	4.9	32.9	345.4	292.1
PEEK-1-TT	NO	47.7	6.1	32.0	346.0	303.5
PEEK-2-TT	NO	48.2	8.2	30.8	345.5	303.5
PEEK-3-TT	NO	48.1	6.0	32.4	346.0	303.4
NANO-1-TT	NO	43.1	4.1	33.3	345.2	292.0
NANO-2-TT	NO	44.5	5.8	33.1	345.2	292.2
NANO-3-TT	NO	44	5.1	33.2	345.8	292.7

NO, not observed

The earlier degradation of the PEEK nanocomposite with respect to the neat PEEK could have been due to the presence of the HA, which could have triggered degradation reactions in PEEK during heating.

Characterization of the Injection-Molded Samples. Figure 4 shows PLOM micrographs of the injection-molded PEEK and nanocomposite, processed under condition 2, before and after the thermal treatment. All of the other injection-molded samples had similar morphologies. We observed that the samples without the thermal treatment had a well-defined skin and core morphology. In the pure PEEK, the skin was transparent, whereas in the nanocomposite, the skin was opaque (crystalline). After the thermal treatment, however, the skin of both samples almost disappeared, because of the increase in the crystallinity.

The thickness of the skin of all of the samples was measured, and it is shown in Table III; we observed that, as expected, the lower Q was, the lower the shear rate and the higher the time for the beginning of the flow-induced crystallization to occur were, as confirmed by other works.[30–32] Therefore, the thickness of the frozen skin layer was higher. Also, the higher thermal conductivity of the nanocomposite contributed to the increase in the skin. On the other hand, in general, the thickness of the skin of the pure PEEK injected under the same conditions was lower than that of the nanocomposite because of its lower viscosity.

Table III also shows the thermal parameters of the injection-molded samples calculated by DSC. We observed that the thermal treatment increased the crystallinity of the samples, as expected. All of the samples also showed cold crystallization, even the thermally treated ones; this indicated that the thermal treatment was not enough to attain the highest amount of crystallinity in the samples. The addition of HA slightly increased the amount of crystallinity of the thermally and non thermally treated samples; this was in contrast to other results.[32] The amount of crystallinity was also dependent of the injection-molding conditions, as expected; for example, PEEK and the nanocomposite injected under condition 1 (lowest Q) had the lowest X_{c_DSC} because a low Q favored the formation of a thicker skin (frozen layer) and a low X_{c_DSC}.

T_m of the injection-molded samples was not affected by any of the studied factors (amount of HA, thermal treatment, and injection-molding conditions). However, T_c was affected by the presence of the HA, as was already observed in the 90/10-ext sample (the extruded nanocomposite). As we said before and as has been confirmed by some authors,[33] in the DSC equipment, crystallization is slow and quiescent, and a retardation effect can occur, in which the nanoparticles of HA retard the diffusion of the polymeric chains. This makes nucleation and crystal growth more difficult and delays crystallization. Another work of ours[32] on optical monitoring during the injection molding of polypropylene (PP) and MMT nanocomposites showed that the PP/MMT nanocomposites had higher induction times for the beginning of crystallization than the pure PP; this confirmed the retardation effect in the growth rate promoted by the MMT nanoparticles.

Figure 5 shows the WAXD spectra of all of the injection-molded samples. We observed that the PEEK samples without the thermal treatment [Figure 5(a)] displayed small peaks at 18.8, 20.7, 22.9, and 28.9°; these corresponded to the (110), (111), (200), and (211) crystalline planes of the PEEK.[34] The red dots in the online figure designate the crystalline peaks of HA. Because the X-ray penetration on the sample was mainly limited to the surface,[28] we concluded that the skin of the samples had a very low amount of crystallinity. On the other hand, after the thermal treatment, as shown in Figure 5(b), the peaks related to the crystalline structure of the PEEK were sharper and narrower than in the nonannealed samples. Therefore, the skin showed an increase in crystallinity after the thermal treatment.

Mechanical Properties of the Injection-Molded Samples

The tensile stress versus strain curves of the injection-molded samples are shown in Figure 6, whereas the values of the UTS, E, stress at break (σ_b), and strain at break (ε_b) are shown in Table IV.

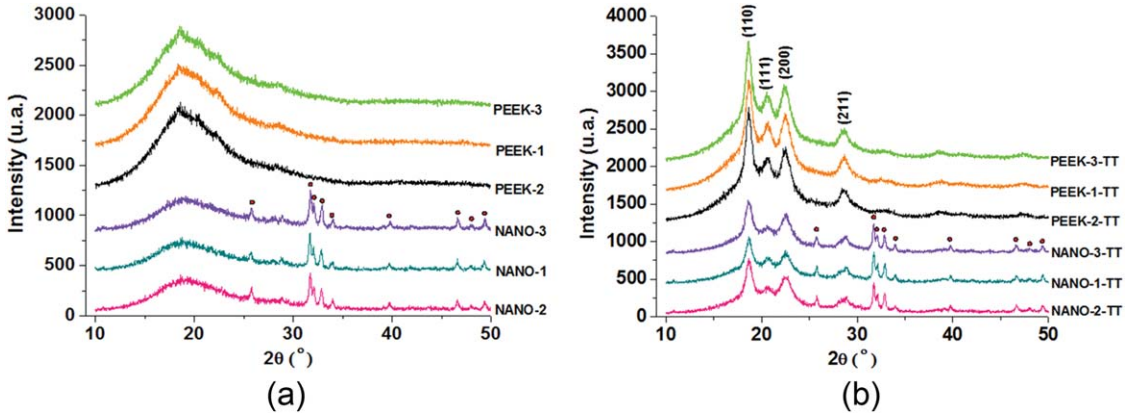

Figure 5. WAXD diffractograms of the injection-molded samples (a) before and (b) after the thermal treatment. The red dots in the online figure designate the peaks of HA. [Color figure can be viewed in the online issue, which is available at wileyonlinelibrary.com.]

Before the thermal treatment, we observed that the addition of HA to PEEK increased E (∼12%) but highly decreased σ_b (∼30%) and ε_b (∼88%) of the nanocomposites, whereas UTS was not modified by the addition. After the thermal treatment, again the nanocomposites had an increase in E (∼15%), decreases in σ_b (∼15%) and ε_b (∼92%), and no modification of UTS with respect to the thermally treated pure PEEK. However, in a comparison of the non thermally treated and thermally treated nanocomposites, we observed that the thermal treatment increased UTS (∼9%), E (∼11%), and σ_b (∼6%) and decreased ε_b (∼44%).

The increase in UTS after the thermal treatment was very important because this stress, combined with a safety factor, represented the maximum solicitation stress that could be applied during use. After this value was attained, plastic deformation was significant and not uniform. Therefore, the addition of 10 wt % HA to PEEK produced a nanocomposite with a UTS within the range of cortical bone but with a lower E.[35] On the other hand, the UTS and E of the PEEK/HA nanocomposites were much higher than the UTS and E of trabecular bone.[35] We believe that besides increasing the crystallinity, the thermal treatment also strengthened the interphase HA/PEEK by extending or stretching the PEEK macromolecules at the surface of HA (and thus increasing E and σ_b but decreasing ε_b), like a Mullins effect (but with a contrary influence on E), as shown in scheme of Figure 7(a).

The Izod impact strength of the injection-molded samples is also shown in Table IV. We observed that:

1. The thermal treatment decreased the impact strength of all of the samples, probably because of an increase in the crystallinity.
2. In the non thermally treated samples, the addition of HA to PEEK did not change the impact strength (with the exception of samples PEEK-3 and NANO-3, in which an increase in the impact strength was observed).
3. In the thermally treated samples, the addition of HA to PEEK again did not change the impact strength (with the exception again of samples PEEK-3–TT and NANO-3–TT, in

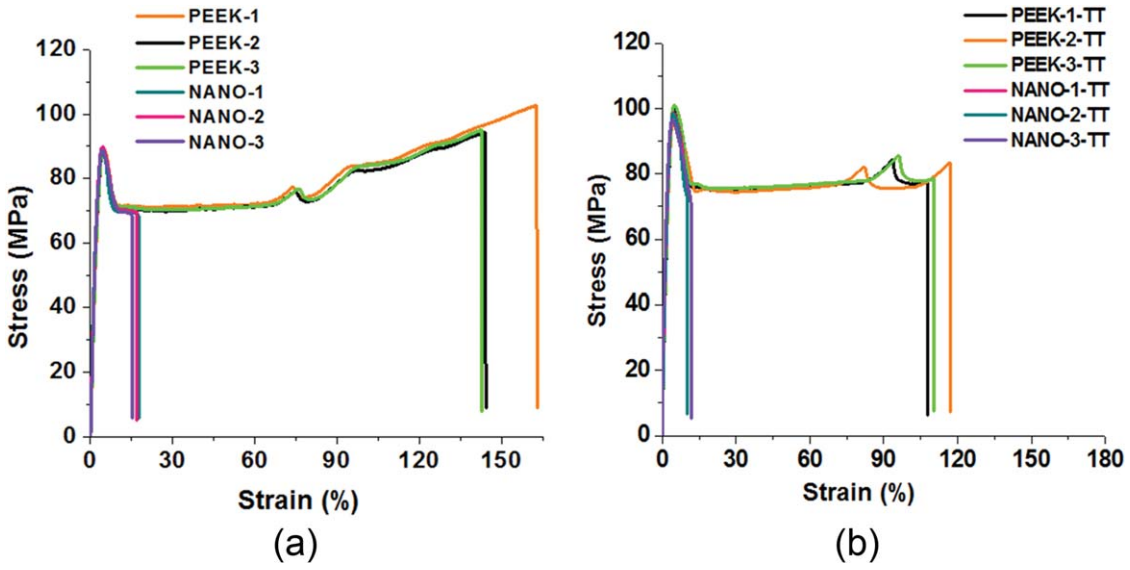

Figure 6. Tensile stress versus strain of the injection-molded samples (a) without and (b) with the thermal treatment. [Color figure can be viewed in the online issue, which is available at wileyonlinelibrary.com.]

Table IV. Mechanical Properties of the Injection-Molded Samples

Sample	UTS (MPa)	*E* (GPa)	σ_b (MPa)	ε_b (%)	IZOD impact strength (J/m)
PEEK-1	89.1 ± 0.3	3.5 ± 0.1	100.5 ± 4.9	161.5 ± 9.5	52.38 ± 3.32
PEEK-2	87.6 ± 0.2	3.5 ± 0.1	95.7 ± 3.1	148. 8 ± 8.2	51.33 ± 2.45
PEEK-3	88.3 ± 0.3	3.6 ± 0.2	95.5 ± 0.9	144.3 ± 2.8	51.43 ± 1.89
NANO-1	88.8 ± 0.2	3.9 ± 0.1	68.7 ± 0.6	19.0 ± 6.3	54.30 ± 2.67
NANO-2	90.0 ± 0.4	3.9 ± 0.1	68.7 ± 1.4	18.8 ± 6.4	50.19 ± 2.03
NANO-3	89.1 ± 0.2	4.1 ± 0.2	68.5 ± 0.5	14.8 ± 3.1	56.45 ± 1.22
PEEK-1-TT	98.5 ± 0.7	4.0 ± 0.03	87.5 ± 6.8	133.4 ± 20.7	44.77 ± 4.35
PEEK-2-TT	98.6 ± 0.9	3.8 ± 0.1	83.3 ± 8.0	111.8 ± 24.8	45.12 ± 3.70
PEEK-3-TT	98.1 ± 0.9	3.8 ± 0.1	87.5 ± 5.7	124.7 ± 10.7	40.38 ± 1.81
NANO-1-TT	98.2 ± 0.4	4.4 ± 0.1	73.2 ± 0.2	9.7 ± 0.5	42.48 ± 1.58
NANO-2-TT	98.5 ± 0.9	4.4 ± 0.04	74.0 ± 2.4	9.7 ± 0.5	44.68 ± 3.02
NANO-3-TT	96.4 ± 0.4	4.4 ± 0.1	71.7 ± 2.0	10.3 ± 2.1	44.31 ± 3.31
Cortical bone[26]	50–150	7–30	—	—	—
Trabecular bone[26]	10–20	0.05–0.5	—	—	—

which an increase in the impact strength was again observed).

These last results suggest that no formation of large agglomerates of HA (which could concentrate the stress and decrease the impact resistance[36]) occurred. Sample NANO-3 (the nanocomposite of PEEK and 10 wt % HA) injection-molded at a high *Q* (conditions 3) had the best impact resistance of all of the samples; this was probably due to high orientation along the samples promoted by the high shear rates.

Micrographs of the fracture surface are also shown in Figure 7. Because no compatibilization agent was used, some particles did not adhere to PEEK, as shown in Figure 7(b), whereas in other

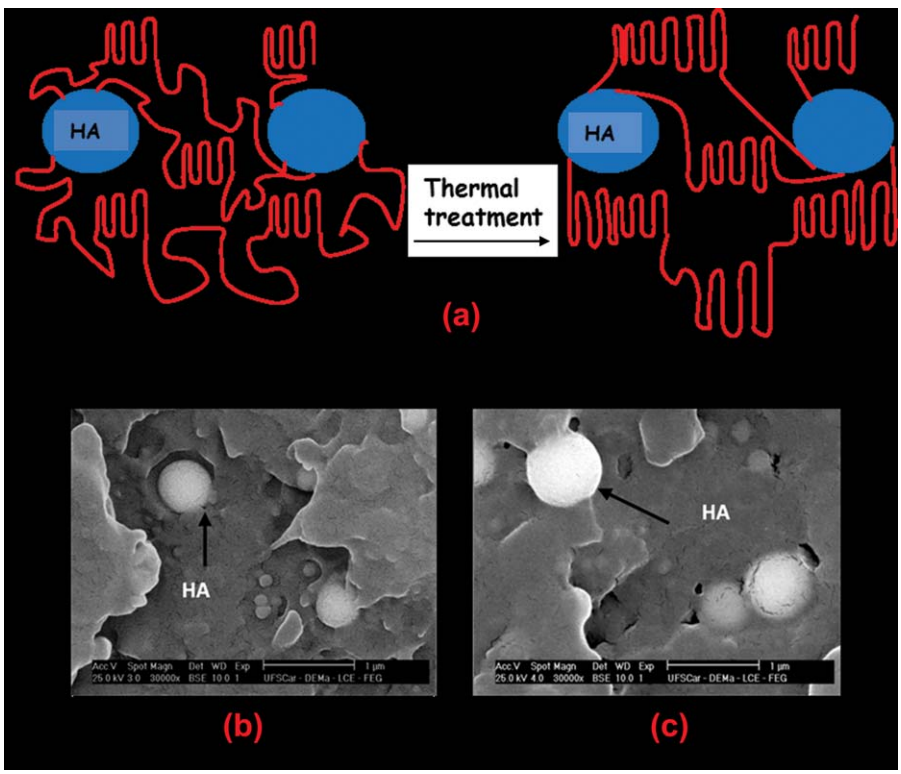

Figure 7. (a) Scheme of the contribution of the interphase HA nanoparticle–PEEK macromolecules to the increase in *E* and σ_b, (b) HA nanoparticle detached from the PEEK, and (c) HA nanoparticle attached to the PEEK. [Color figure can be viewed in the online issue, which is available at wileyonlinelibrary.com.]

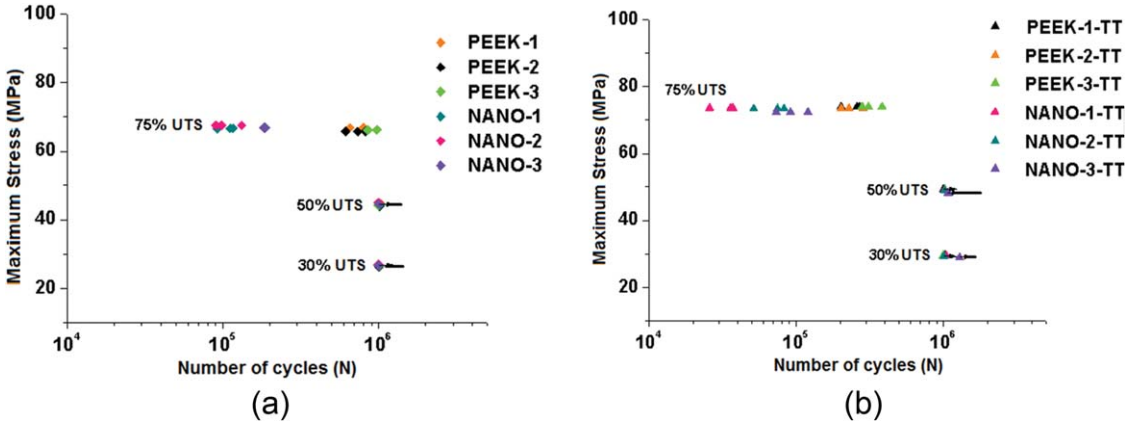

Figure 8. SN curves for the injection-molded samples (a) without and (b) with thermal treatment. The black arrows indicate that the material did not fail after it reached 10^6 cycles. [Color figure can be viewed in the online issue, which is available at wileyonlinelibrary.com.]

regions of the fracture surface, adhesion between HA and PEEK was observed, as shown in Figure 7(c). Debonding can be damaging for load transfer; therefore, compatibilization studies with silane coupling agents between HA nanoparticles and PEEK macromolecules are underway,[37] and they seem promising.

Figure 8 shows the SN curves of the samples. During fatigue testing, the temperatures of the samples were 25°C (30% of the UTS), 27°C (50% of the UTS), and 33°C (75% of the UTS). That is, even at a frequency of 10 Hz, the increase in the temperature in the samples was lower than the body temperature (36.5°C) and the PEEK's T_g (143°C).

We observed that all of the samples, with and without thermal treatment, did not fail after the application of maximum stresses of 30 and 50% of the UTS. However, when σ_{max} was 75% of the UTS, all of the samples failed. In the case of the pure PEEK, without thermal treatment, the sample withstood approximately 8.0×10^5 cycles, whereas after the thermal treatment, it withstood 2.7×10^5 cycles. This was a reduction of approximately 38% in the fatigue life. On the other hand, the nanocomposite without thermal treatment withstood approximately 1.1×10^5 cycles, whereas the thermally treated sample withstood 7.5×10^4 cycles. This was a reduction of approximately 31% in the fatigue life. The decrease in the fatigue life was expected because the presence of the nanoparticles created a high amount of interphases within the matrix; this could have initiated and propagated fissures, as proposed by Tang *et al.*[38] Again, particle debonding was crucial for the decrease in the fatigue life; therefore, as said before, compatibilization studies with silane coupling agents between HA particles and PEEK are underway[37] and seem promising.

The thermal treatment also decreased the fatigue life. Saib *et al.*,[39] for example, observed that after a thermal treatment of PEEK notched samples, the ones with the highest amount of crystallinity had the highest crack growth strength; this was probably due to the increase in the orientation and number of crystallites, which required more energy to deform and fracture. On the other hand, in another study, Sobieraj *et al.*[40] observed that most of the fatigue energy was expended to initiate the crack; that is, when the fatigue life was highest, the ratio between the number of cycles necessary to initiate the crack and the number of cycles necessary to propagate the crack was highest. Therefore, we concluded that the increase in the crystallinity after the thermal treatment of PEEK accelerated crack initiation but decreased crack propagation.

Our nanocomposite behaved in a manner similar to cortical bone because it did not fail up to 10^6 cycles when stresses up to 49 MPa were applied, but it failed at 25,905 and 187,293 cycles when stresses of 67 and 73 MPa were applied instead.

Figure 9 shows the dynamic mechanical analyses of the samples, and Table V shows the values of E', E'', tan δ at 37°C, and T_g for all of the samples.

Before the thermal treatment, we observed that at 37°C, the addition of HA to PEEK increased E' by an average of 15% and E'' by approximately 28% without changing the T_g (~147°C). This last behavior was probably due to the low chemical interaction between the PEEK macromolecules and HA, as observed by Lai *et al.*[41] After the thermal treatment, at 37°C, there was again an increase in E' of approximately 15% and one in E'' of approximately 13% without a change in T_g (~161°C) with the addition of HA to PEEK. In a comparison of the non thermally treated and thermally treated samples, we concluded that the thermal treatment increased E' by approximately 16% and E'' by approximately 79% in the pure PEEK, whereas in the nanocomposite, an increase of E' of approximately 17% and one in E'' of approximately 44% occurred. That is, the thermal treatment improved the viscoelastic properties of both materials. We also observed that before the thermal treatment, a slight increase in E' and an additional small peak in E'' after T_g were observed. This was probably due to the further crystallization of the samples during dynamic testing. After the thermal treatment, however, both behaviors disappeared, as also observed in other studies.[42]

It is worthwhile to recall that tan δ (E''/E') is a measure of the damping capability of the material. E'' is proportional to the amount of dissipated energy, whereas E' is proportional to the elasticity of the material. The dissipation of energy in a material occurs by many mechanisms, and molecular internal friction is one of them. In a composite, the dissipation of energy can also

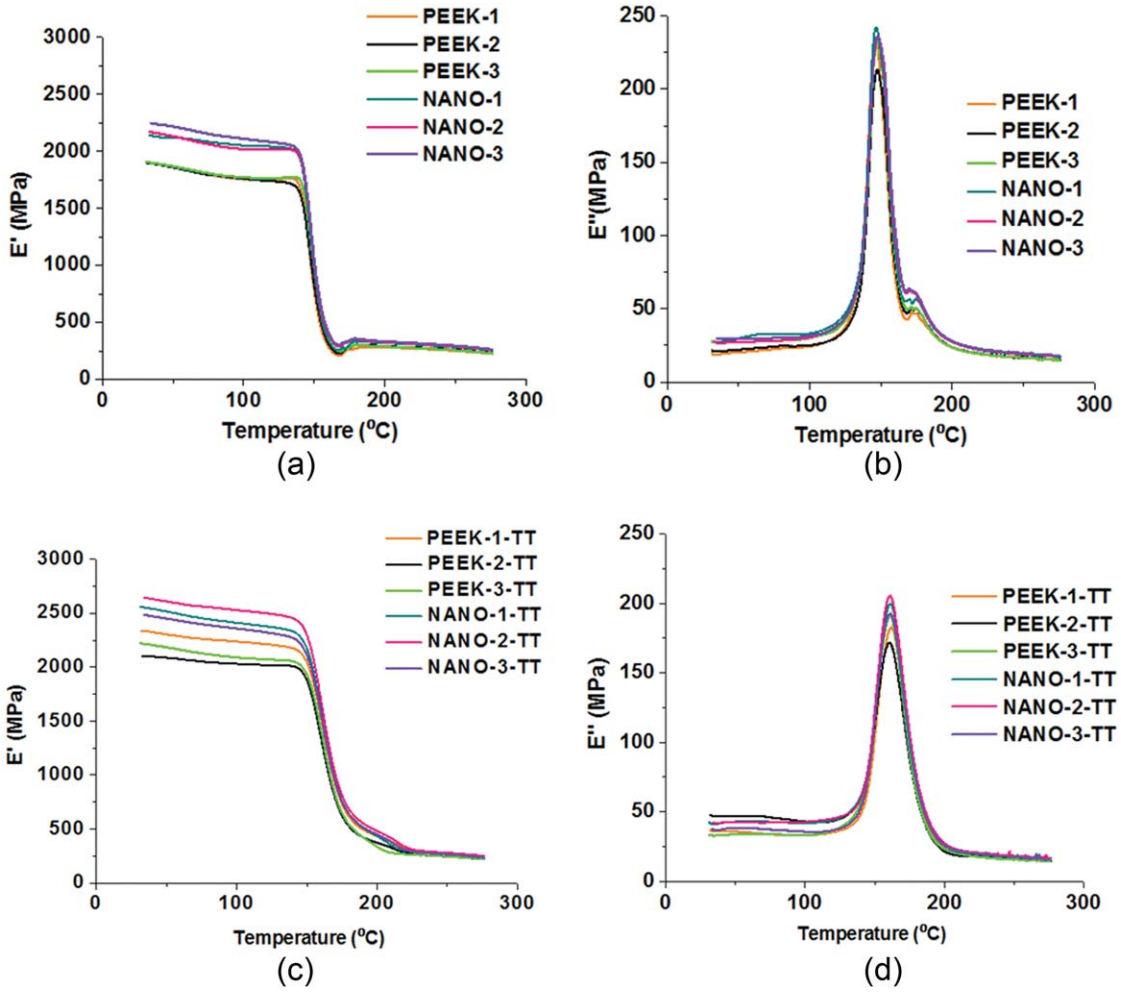

Figure 9. E' and E'' as a function of the temperature of the injection-molded samples (a,b) without and (c,d) with thermal treatment. [Color figure can be viewed in the online issue, which is available at wileyonlinelibrary.com.]

originate from the friction occurring in the polymer matrix–particle interphase. A high damping material (e.g., elastomers), therefore, will have a high tan δ; however, very high damping can decrease the dimensional stability of the material. This is undesirable in implants. The highest damping was found in sample PEEK-2–TT, and the lowest was found in sample PEEK-

Table V. E', E'', Tan δ (at 37°C), and T_g Values of the Injection-Molded Samples

Sample	E' (GPa) at 37°C	E'' (MPa) at 37°C	Tan δ at 37°C	T_g (°C) [peak of E'']
PEEK-1	1.89	18.71	0.0098	146.8
PEEK-2	1.89	20.57	0.0108	148.3
PEEK-3	1.90	26.60	0.0140	147.8
NANO-1	2.13	27.17	0.0127	147.0
NANO-2	2.16	26.46	0.0122	148.2
NANO-3	2.24	29.1	0.0129	147.5
PEEK-1-TT	2.33	35.31	0.0151	162.6
PEEK-2-TT	2.09	46.30	0.0221	161.4
PEEK-3-TT	2.21	32.60	0.0147	161.0
NANO-1-TT	2.54	40.99	0.0161	161.7
NANO-2-TT	2.63	41.44	0.0157	161.3
NANO-3-TT	2.47	36.47	0.0147	161.0

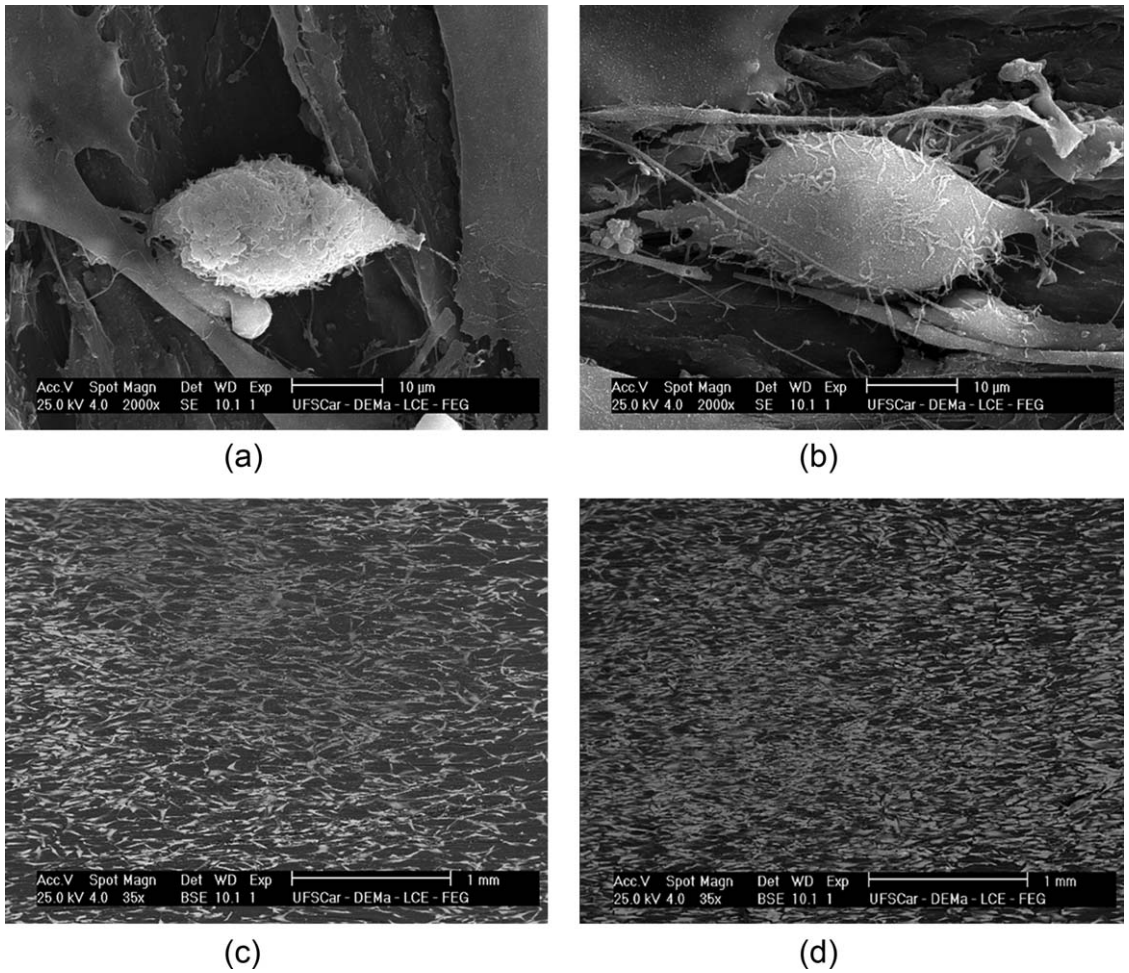

Figure 10. h-ASCs on the surface of the injection-molded samples: (a,c) PEEK and (b,d) PEEK/HA. The micrographs were taken after 5 days of culturing.

1. That is, the addition of HA and the thermal treatment increased the damping capability of PEEK.

Cell Adhesion

The adhesion and proliferation of the h-ASCs were observed in the PEEK and PEEK/HA nanocomposite, as shown in Figure 10(a,b). The presence of the HA seemed to enhance the cell proliferation in the nanocomposite compared to the pure PEEK, as shown in the micrographs of Figure 10(c,d), which were taken after 5 days of culturing. The measured area occupied by the h-ASCs and other cellular materials in the PEEK sample was 49%, whereas that in the PEEK/HA sample was 68%. This result suggest, therefore, that the HA helped the h-ASCs in their adhesion, proliferation, and growth on the surface of the nanocomposite, as already observed in other works.[23]

CONCLUSIONS

Nanocomposites of PEEK with 10 wt % HA were produced by twin-screw extrusion and injection molding; to increase X_{c_DSC}, the injection-molded samples were annealed. When HA was added to PEEK, an increase in E but a decrease in σ_b and ε_b were observed without modification of the UTS. On the other hand, the thermal treatment highly improved these tension mechanical properties. The UTS and E of the nanocomposite were found to be much higher than the UTS and E of trabecular bone. The impact strength of the PEEK was not modified by the addition of HA, whereas the thermal treatment decreased this strength, as expected. A decrease in the fatigue life was also observed when HA was added to the PEEK and also when the samples were thermally treated. All of the samples, with and without thermal treatment, did not fail after the application of stresses of 30 and 50% of the UTS. However, when the applied stress was 75% of the UTS, all of the samples failed. This behavior was similar to the behavior in fatigue of cortical bone. The poor interphase, which promoted debonding between the HA nanoparticles and the PEEK macromolecules, was probably the cause for the low improvement in the mechanical strength; however, studies with silane coupling agents are underway[37] and seem promising.

Because of the presence of the HA, the proliferation of the h-ASCs was higher in the nanocomposite than in the pure PEEK.

ACKNOWLEDGMENTS

The authors thank Fundação de Amparo à Pesquisa do Estado de São Paulo (FAPESP) and Coordenação de Aperfeiçoamento de Pessoal de Nível Superior (CAPES) for financial aid.

REFERENCES

1. Hahna, B. D.; Parka, D. S.; Choi, J. J.; Ryua, J.; Yoona, W. H.; Choi, J. H.; Kima, J. W.; Ahna, C. W.; Kimb, H. E.; Yoonc, B. H. *Appl. Surf. Sci.* **2013**, *283*, 6.
2. Kim, M. M.; Boahene, K. D. O.; Byrne, P. *J. Arch. Facial Plast. Surg.* **2009**, *11*, 53.
3. Webster, T. J.; Patel, A. A.; Rahaman, M. N.; Bal, B. S. *Acta Biomater.* **2012**, *8*, 4447.
4. Chi, M. H.; Tsou, H. K.; Chung, C. J.; He, J. L. *Thin Solid Films* **2013**, *549*, 98.
5. Kurtz, S. M.; Devine, J. N. *Biomaterials* **2007**, *28*, 4845.
6. Jalbert, F.; Boetto, S.; Nadon, F.; Lauwers, F.; Schmidt, E.; Lopez, R. *J. Cranio Maxillofac. Surg.* **2014**, *42*, 141.
7. Oréfice, R. L. Biomateriais: Fundamentos e Aplicações; Cultura Médica: Rio de Janeiro, **2006**.
8. Abu Bakar, M. S.; Cheang, P.; Khor, K. A. *Compos. Sci. Technol.* **2003**, *63*, 421.
9. Abu Bakar, M. S.; Cheng, M. H. W.; Tang, S. M.; Yu, S. C.; Liao, K.; Tan, C. T.; Khor, K.; Cheang, P. A. *Biomaterials* **2003**, *24*, 2245.
10. Zhao, Y.; Wong, H. M.; Wang, W.; Li, P.; Xu, Z.; Chong, E. Y. W.; Yan, C. H.; Yeung, K. W. K.; Chu, P. K. *Biomaterials* **2013**, *34*, 9264.
11. Wang, L.; Weng, L.; Song, S.; Zhang, Z.; Tian, S.; Ma, R. *Mater. Sci. Eng. A* **2011**, *528*, 3689.
12. Webster, T. J.; Ergun, C.; Doremus, R. H.; Siegel, R. W.; Bizios, R. *Biomaterials* **2000**, *21*, 1803.
13. Webster, T. J.; Schadler, L. S.; Siegel, R. W. *Tissue Eng.* **2001**, *7*, 291.
14. Yao, C.; Perla, V.; McKenzie, J. *J. Biomed. Nanotechnol.* **2005**, *1*, 68.
15. Perla, V.; Webster, T. J. *J. Biomed. Mater. Res.* **2005**, *75*, 356.
16. Roeder, R. K.; Converse, G. L.; Kane, R. J.; Yue, W. *Biol. Mater. Sci.* **2008**, *60*, 38.
17. Kane, R. J.; Converse, G. L.; Roeder, R. K. *J Mech. Behav. Biomed. Mater.* **2008**, *1*, 261.
18. Wang, L.; Weng, L.; Song, S.; Sun, Q. *Mater. Lett.* **2010**, *64*, 2201.
19. Ma, R.; Weng, L.; Bao, X.; Ni, Z.; Song, S.; Cai, W. *Mater. Lett.* **2012**, *71*, 117.
20. Silva, A. B.; Marini, J.; Gelves, G.; Sundararaj, U.; Gregório, R., Jr.; Bretas, R. E. S. *Eur. Polym. J.* **2013**, *49*, 3318.
21. Lu, C.; Mai, Y. W. *Phys. Rev. Lett.* **2005**, *95*, 1.
22. Lorenz, C. D.; Ziff, R. M. *J. Chem. Phys.* **2001**, *114*, 3659.
23. Ribeiro Neto, W. A.; Pereira, I. H. L.; Ayres, E.; de Paula, A. C. C.; Averous, L.; Góes, A. M.; Oréfice, R. L.; Bretas, R. E. S. *Polym. Degrad. Stab.* **2012**, *97*, 2037.
24. Beatrice, C. A. G.; Alves, R. M. V.; Branciforti, M. C.; Bretas, R. E. S. *J. Appl. Polym. Sci.* **2010**, *116*, 3581.
25. Hay, J. N.; Kemmish, D. *J. Polymer* **1987**, *28*, 2047.
26. KetaSpire® KT-820; Technical Data Sheet; Solvay Specialty Polymers, **2011**; p 1.
27. Blundell, D. J.; Osborn, B. N. *Polymer* **1983**, *24*, 953.
28. Farah, M.; Bretas, R. E. S. *J. Appl. Polym. Sci.* **2004**, *91*, 3528.
29. Favaro, M. M.; Rego, B. T.; Branciforti, M. C.; Bretas, R. E. S. *J. Polym. Sci. Part B: Polym. Phys.* **2010**, *48*, 113127.
30. Marinelli, A. L.; Farah, M.; Bretas, R. E. S. *J. Appl. Polym. Sci.* **2006**, *99*, 563.
31. Favaro, M. M.; Marinelli, A. L.; Farah, M.; Bretas, R. E. S. *Polym. Eng. Sci.* **2008**, *48*, 257.
32. Moretti, F.; Favaro, M. M.; Branciforti, M. C.; Bretas, R. E. S. *Polym. Eng. Sci.* **2010**, *50*, 1326.
33. Li, L.; Li, C. Y.; Ni, C.; Rong, L.; Hsiao, B. *Polymer* **2007**, *48*, 3452.
34. Díez-Pascual, A. M.; Naffakh, M.; Gómez, M. A.; Marco, C.; Ellis, G.; Martínez, M. T.; Ansón, A.; González-Domínguez, J. M.; Martínez-Rubi, Y.; Simard, B. *Carbon* **2009**, *47*, 3079.
35. Bonfield, W.; Wang, M.; Tanner, K. E. *Acta Mater.* **1998**, *46*, 2509.
36. Knör, N.; Walter, R.; Haupert, F. *J. Thermoplast. Compos. Mater.* **2011**, *24*, 185.
37. Marcomini, A. L.; Rego, B. T.; Bretas, R. E. S. Presented at XIV Latin American Symposium in Polymers (SLAP)—XII Ibero—American Congress in Polymers (CIP), Porto de Galinhas, Oct **2014**, Pernambuco, Brasil.
38. Tang, S. M.; Cheang, P.; Abu Bakar, M. S.; Khor, K. A.; Liao, K. *Int. J. Fatigue* **2004**, *26*, 49.
39. Saib, K. S.; Evans, W. J.; Isaac, D. H. *Polymer* **1993**, *34*, 3198.
40. Sobieraj, M. C.; Murphy, J. E.; Brinkman, J. G.; Kurtz, S. M.; Rimnac, C. M. *Biomaterials* **2010**, *31*, 9156.
41. Lai, Y. H.; Kuo, M. C.; Huang, J. C.; Chen, M. *Mater. Sci. Eng. A* **2007**, *458*, 158.
42. Malpass, V. E. *Appl. Polym. Symp.* **1969**, *12*, 267.